Signatures of Cross-sectional Width Modulation in Solar Spicules due to Field-aligned Flows

MacKenzie Dover, Fionnlagh; Sharma, Rahul; Korsós, Marianna B.; Erdélyi, Robertus

Published in:
Astrophysical Journal

DOI:
10.3847/1538-4357/abc349

Publication date:
2020

Citation for published version (APA):
MacKenzie Dover, F., Sharma, R., Korsós, M. B., & Erdélyi, R. (2020). Signatures of Cross-sectional Width Modulation in Solar Spicules due to Field-aligned Flows. *Astrophysical Journal*, *905*(1), [72]. https://doi.org/10.3847/1538-4357/abc349

Draft version January 4, 2021
Typeset using LaTeX **twocolumn** style in AASTeX62

Signatures of Cross-Sectional Width Modulation in Solar Spicules due to Field Aligned Flows

Fionnlagh Mackenzie Dover[1] and Rahul Sharma[2]

Marianna B. Korsós[3, 4, 5]

Robertus Erdélyi[1, 4, 5]

[1]*Solar Physics & Space Plasma Research Centre (SP²RC), School of Mathematics and Statistics, The University of Sheffield, Hicks Building, Hounsfield Road, Sheffield, S3 7RH U.K.*

[2]*Space Weather Research Group, Departamento de Física y Matemáticas, Universidad de Alcalá, A-2 km 33,600, 28871 Alcalá de Henares, Madrid, Spain*

[3]*Department of Physics, Aberystwyth University, Ceredigion, Cymru, SY23 3BZ, U.K.*

[4]*Department of Astronomy, Eötvös Loránd University, Pázmány Péter sétány 1/A, H-1117 Budapest, Hungary*

[5]*Gyula Bay Zoltán Solar Observatory (GSO), Hungarian Solar Physics Foundation (HSPF), Petőfi tér 3., Gyula, H-5700, Hungary*

(Received TBC; Revised TBC; Accepted TBC)

Submitted to ApJ

ABSTRACT

We report the first observational detection of frequency modulation in cross sectional width of spicule structures due to field-aligned plasma flows. Cross-sectional width variations were estimated for least superimposed off-limb spicules observed in high-resolution Hα imaging-spectroscopy data. Analysis of estimated cross sectional widths suggest periodic oscillations, concurrent with 2D numerical modelling for a jet structure in a stratified solar atmosphere. Spectral analysis for both observed and simulated cross-sectional widths indicate frequency modulation as noticeable shifts in estimated periodicities during rise and fall phases of field aligned plasma flows in the jet structure. Furthermore, the presence of first overtone in a dynamic/spicular waveguide is also evident in both the observed and the simulated jet structures. These harmonics can be important tool for future chromospheric magnetoseismology investigations and applications to dynamic waveguides (like spicules).

Keywords: Sun: chromosphere – oscillations – spicules

1. INTRODUCTION

Spicules are thin, grass-like features that are routinely observed in the lower solar atmosphere as dark (on-disk) or bright (at limb) structures, primarily in cool/chromospheric spectral lines (e.g., Hα, Ca II H & K, He I D3). These localised features effectively trace the chromospheric magnetic field concentrations in spite of the likely role of the neutrals at spicular temperatures and are a focus of many studies for their potential role in balancing the radiative losses and heating at the chromosphere-corona interface (Tsiropoula et al. 2012).

Corresponding author: Robertus Erdélyi
robertus@sheffield.ac.uk

Observations suggest that spicules generally emanate near the (inter)granulation lanes and remain subject to magnetohydrodynamic stresses (MHD) at their footpoint. The associated motions, irrespective of whether turbulent or coherent, become channelized through the spicule structure and are well reflected in their observed dynamic behavior. Broadly, spicule kinematics can be categorized in three major domains, viz., radially transverse, field-aligned and torsional, which have been extensively examined and interpreted in terms of discrete MHD wave modes (see review: Zaqarashvili & Erdélyi 2009).

Ubiquitous transverse displacements in spicule features were interpreted as the $m = 1$, kink MHD wave mode by previous studies, e.g. (Kukhianidze et al. 2006; De Pontieu et al. 2007; Ebadi & Ghiassi 2014;

Sharma et al. 2017). Similar dynamic behavior is also found prevalent in on-disk spicule-counterparts, commonly known as Rapid Blue/Red Shifted Excursions (RBE,RREs: Rouppe van der Voort et al. 2009). Field-aligned motions are primarily associated with mass flows, and common to many jet-like phenomenon, were reported in mottles (Loughhead 1974), on-disk RBE/RREs (Sekse et al. 2013) and off-limb spicules (Pereira et al. 2012). Axisymmetric torsional (rotationally transverse) motions in spicules were claimed to be observed in terms of $m = 0$ torsional Alfvén wave mode by De Pontieu et al. (2012), however, it must be noted that the observations used to make this particular mode identification could also be due to perturbations in ambient chromospheric environment by spicule motions (Goossens et al. 2014; Sharma et al. 2017).

Though much attention was given to the identification and study of transverse (kink and torsional Alfvén) wave modes, the observations of cross-sectional width variations remained elusive, largely due to pertinent difficulties with observations of jet-like chromospheric features. **The presence of cross-sectional width variations in thin magnetic flux tube structures, as a possible consequence of $m = 0$ MHD sausage and/or $m = 2$ fluting modes, were postulated in earlier theoretical studies (Ziegler & Ulmschneider 1997a,b; Ruderman et al. 2010).** A few observations of periodic cross-sectional width variations were limited to on-disk fibril structures. Concurrent transverse and cross-sectional width variations were reported as coupled kink and sausage wave modes by Jess et al. (2012) and Morton et al. (2012). Similar observations for cross-sectional width and intensity oscillations in on-disk slender chromospheric fibrils were reported by Gafeira et al. (2017) and interpreted as MHD sausage wave modes. Moreover, an ensemble of coupled transverse, cross-sectional width and axisymmetric torsional motions were reported in off-limb spicules by Sharma et al. (2018), which were interpreted as nonlinear kink wave mode.

It must, however, be noted that spicules are essentially jet-like features where mass flows along their magnetic field are predominant with bulk velocities of the range of 25-100 km/s (Beckers 1972; Sterling 2000; Pereira et al. 2012). Such bulk velocities may even have a dominant effect on the waves that are present in spicular structures. Plasma flows will interact with the oscillatory modes of spicules, e.g. periodic motions along or anti-parallel to the bulk motion will be affected differently. Wave motions in steady waveguides have been investigated in the past in a few theoretical studies (Narayanan 1991; Nakariakov & Roberts 1995; Terra-Homem et al. 2003; Soler et al. 2008) for different (slab/cylindrical) geometries. It was concluded that mass flows can generate shift in frequencies for confined MHD waves and can influence the wave propagation even causing resonant flow instabilities, depending upon the direction and strength of mass flows. Though, possible effects of mass flows on wave periodicities/propagation were known theoretically, it still requires observational verification in highly localised dynamic waveguides such as solar spicules.

Here, we examine the cross sectional width variations in off-limb spicule structures and compare the observed dynamical behavior with 2D MHD numerical simulations. The prime objective of the numerical setup is to mimic the fundamental kinematic behavior of a jet (flows, cross sectional widths) in a stratified solar atmosphere and to investigate the underlying physical mechanisms. Spectral analysis of cross-sectional width deformations during the rise and fall phases of plasma in both the observed and simulated spicule features are examined to better understand the possible role of field-aligned mass flows in modulating the observed periodicities.

2. DATA AND ANALYSIS

2.1. *Observational Data*

Data used in our investigation were taken by using the CRisp Imaging SpectroPolarimeter (CRISP) at the Swedish 1-m Solar Telescope (SST: Scharmer et al. 2008) on La Palma. The Hα imaging-spectroscopic data of 07:15-07:48 UT, June 21, 2012, targeted an active region (AR) NOAA AR11504 with two sunspots at the limb position (heliocentric coordinates w.r.t the disk center, hereby denoted as: Θ = 893, Φ = -250). The AR was scanned using 31 equally spaced line positions with 86 mÅ, steps from -1.376 to +1.29 Å, relative to the line center, along with the additional 4 positions in the far blue wing from -1.376 to 2.064 Å. Following data acquisition, post-processing of data was carried out using the Multi-Object Multi Frame Blind Deconvolution (MOMFBD; van Noort et al. 2005) image restoration algorithm. Also, standard procedures available in the image pipeline for CRISP data (de la Cruz Rodríguez et al. 2015) including differential stretching and removal of dark- and flat-fielding were implemented.

The final science-grade data of ∼30 min duration had a pixel size of 0.059″ (∼43 km), angular-resolution of 0.13″ (∼95 km), and the cadence of 7.7 sec. Following the the Nyquist criterion, the temporal-resolution of the dataset allowed the detection of MHD wave modes with periodicities over 15.4 sec. Candidate spicule(s) for our study (Table 1) were identified as high-intensity structures with least possible superimposition by any other surrounding features during their visible lifetime in an observed passband. The identified spicule structures have an average lifetime of 118 s in a particular line-scan position from the Hα line-center. **It must be noted that spicules tend to evolve in multiple passbands during their much longer (500-800 s) lifetimes (Pereira et al. 2014). Further, the observed features have an average length of** $\sim 3\pm$**.36**

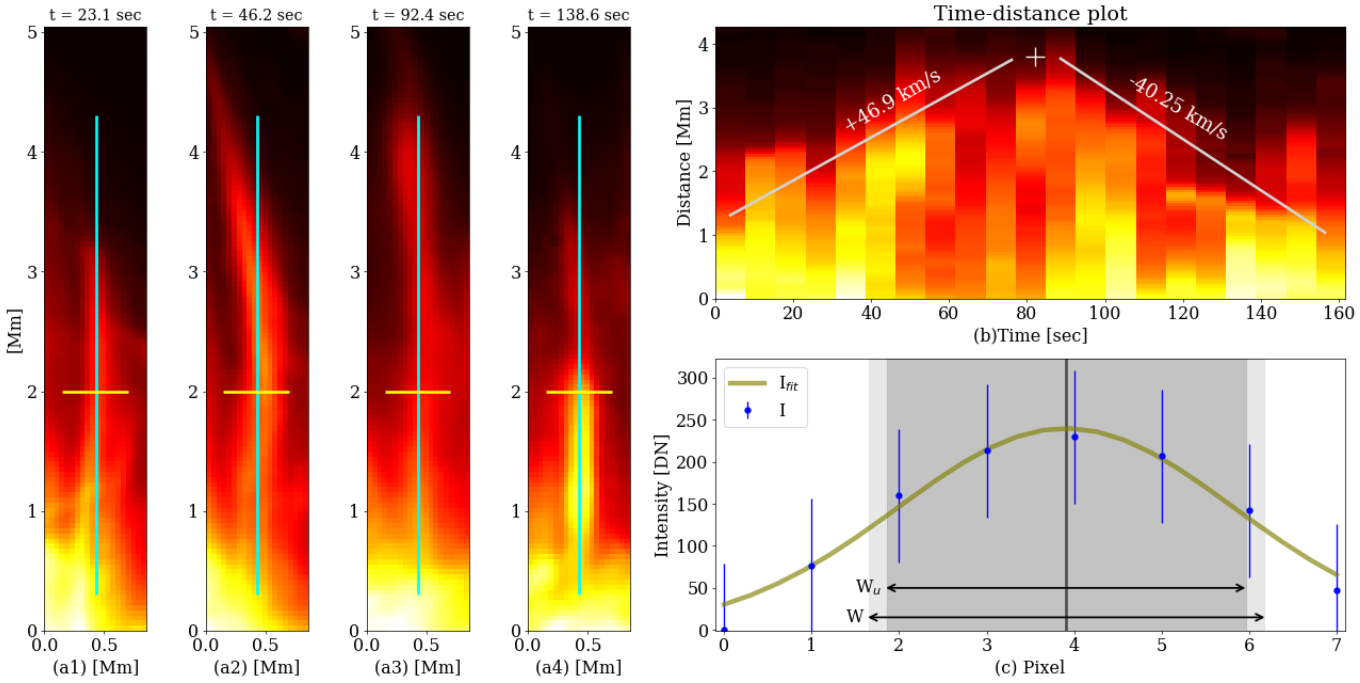

Figure 1. Panels (a1) – (a4) show the temporal evolution of candidate spicule feature (SP:A) in Hα passband at four instances, with positions of vertical (cyan) and horizontal (yellow) slits used for the estimation of field-aligned mass flows and cross-sectional width respectively. Panel (b) shows the time-distance plot from vertical slit on the spicule, highlighting the rise- and fall-phases of field-aligned mass flows. The maximum height attained by the visible plasma is marked with '+' symbol, along with estimated velocities (+46.9 km/s, 40.25 km/s). Bottom panel (c) shows an example of Gaussian fit for intensity magnitudes for horizontal slit location (marked as yellow line on (a1) – (a4)), with error bars, estimated as the standard deviation for intensity values. Vertical black line marks the position of the amplitude of Gaussian fit, while shaded-regions mark average/unperturbed width (W_u) during spicule lifetime and perturbed/instantaneous width (W).

Table 1. Summary of observed physical characteristics of candidate spicule structures along with estimated periodicities during rise-, fall- and overall-phases. Physical and spectral parameters of simulated jet structure are also provided for a comparison between observed and simulated case(s).

Spicule	Lifetime	Length	Apex-height	Unperturbed Width	Periodicity (sec)		
	(sec)	(Mm)	(Mm)	(km)	Rise-phase	Fall-phase	Overall
SP:A	161.7	3.8	5.3	176.0	27.0	16.0	17.0
SP:B	92.4	2.2	4.8	134.6	22.5	27.4	24.7
SP:C	100.1	2.8	4.4	122.8	41.2	31.3	48.8
Simulated jet	471	8.0	8.0	350.0	70.0	30.0+68.0	32.0+65.0

Mm with apex reaching up to an average height of 4.83 Mm. An example of an identified spicule is given in Figure 1(a1)-(a4)), which is presented in detail for field-aligned plasma motions (Fig.1(b)) and its associated role in modulating the cross-sectional widths (Fig.1(c)).

2.2. *Numerical Simulation*

To simulate solar jets numerically, we used grid-adaptive MPI-AMRVAC version 2.0 software developed by e.g. Tóth (1996); Keppens et al. (2012); Porth et al. (2014); Xia et al. (2017). The MHD equations are solved in a 2D setting in a stratified atmosphere in the vertical direction with the non-uniform temperature profile of

$$T_0(y>0) = T_{ch} + \frac{T_c - T_{ch}}{2}\left[\tanh\left(\frac{y-y_{tr}}{w_{tr}}\right)+1\right]. \quad (1)$$

Where y is the vertical position, $T_0(0) = T_{ch} = 8\times 10^3$ K ($T_c = 1.8\times 10^6$ K) is the chromospheric (coronal) temperature and $y_{tr} = 2$ Mm ($w_{tr} = 0.02$ Mm) is the TR height (width).

The simulation box is 50 Mm × 30 Mm with a level one resolution of 32 × 24. Maximum mesh refinement level is set to 7, to achieve a spatial resolution of ∼ 12 km × 10 km. Unidirectional grid stretching is applied in the vertical direction from the origin, where the grid cells change by a factor of 1.1 from cell to cell. This minimises reflection from the top boundary as upward traveling signals become progressively diffusive. For spatial and temporal discretisation the Harten-Lax-van Leer (HLL) solver (Harten et al. 1983) and a third-order Čada limiter (Čada & Torrilhon 2009) are used, respectively. The CFL number is set to 0.8 and the GLM-MHD method is applied to maintain $\boldsymbol{\nabla} \cdot \boldsymbol{B} = 0$, where $\boldsymbol{B}$ is magnetic field strength (Dedner et al. 2002). The right and left boundary conditions are periodic and the lower and upper boundaries act as antisymetric boundary for the velocity components. In addition, the upper boundary ghost cells $\boldsymbol{B}$ are extrapolated assuming zero normal gradient, and density (ρ) and total energy density (e) are determined by gravitational stratification. The lower boundary ghost cells have fixed values for $\rho_0 = 2.34 \times 10^{-4}$ kg m^{-3}, $p_0 = 2.54 \times 10^4$ Pa (converted to conservative form e for temporal advancement) and $\boldsymbol{B}_0 = 50$ G to initial values.

A numerical solar jet is initiated with a momentum pulse

$$v_j(x) = -\frac{A}{2}\left(\tanh\left(\frac{\pi(t-P)}{P} + \pi\right) + 1\right) \exp\left(\frac{x_0 - x}{\Delta x}\right)^2, \quad (2)$$

where v_j is the velocity of the jet, $A = 60$ km s^{-1} is the amplitude of the driver, $P = 300$ sec is the driver time and x_0 is the central location of the jet injection. **The physical parameters (*e.g.*, velocity, length, height, lifetime) of the simulated jet are consistent with observed characteristics of spicules in quiet-Sun and coronal hole environments (Beckers 1972; Pereira et al. 2012, 2014). It should, however, be noted that these parameters for spicular features strongly depends upon the observed passband(s) and regions (coronal hole or quiet-Sun). Here, the simulated jet had a lifetime of ∼470 sec with a maximum height of ∼8 Mm consistent with aforementioned reports for observed spicules characteristics.** The magnetic configuration is uniform in the vertical direction with strength of 50 G, which is consistent with spectropolarimetric estimates for limb spicules (Centeno et al. 2010; Suárez et al. 2015). The output of this configuration is displayed in Figure 2.

2.3. *Wavelet Analysis*

The cross-sectional width of observed spicule features were estimated using the method adopted from Sharma et al. (2018). A single Gaussian function with linear background is used to fit intensity profile across the observed spicules, with estimated FWHM is taken as a measure of cross-sectional width of the feature. For the selected cases in our study, the average estimated FWHM corresponds to 144.4 km, at a height of ∼2 Mm above the visible limb.

The longitudinal and cross-sectional dynamics of numerical jet are examined by employing a tracer quantity that tracks the mass injection and associated motions (Porth et al. 2014). A threshold on the tracer quantity filters out the simulated jet feature from the surrounding region and further helps with the identification of jet boundaries. A horizontal slice on filtered structure facilitate the estimation of width for the particular height and to track the variations over time (see the blue circular markers on Figure 2). **Here, unlike the observed spicule, where FWHM is taken as a proxy for the width of the feature, the cross sectional width of simulated jet indicates overall width of the simulated feature from one edge to the other**. The jet's apex is identified by selecting a single data point that belongs to the jet, with the highest vertical value (see yellow triangular markers on Figure 2). This latter allows for the temporal tracking of the numerical solar jet apex heights and the identification of its rising and falling phases. To perform wavelet analysis, the rise and falling phases are independently detrended with a quadratic polynomial. The detrended data is smoothed to reduce noise by using a moving average with a window size of 15 and 10 for the rising and falling phases, respectively.

Cross-sectional width estimates from both observed and simulated spicule structures were further analyzed using wavelet transform, to understand the nature of periodicities and associated wave physics. To identify any significant periodicities, we constructed wavelet power spectra (WPS) and the associated global power spectrum (GPS) using a software developed by Torrence & Compo (1998). The default Morlet wavelet profile was employed with a two-σ confidence level on cross-sectional width estimates from observations and simulations.

3. RESULTS AND DISCUSSIONS

To understand the role of field-aligned **mass flows on the periodic structural deformations, the width estimates** for an typical observed spicule (Figs.1) were compared with a simulated jet structure. The sample candidate off-limb spicule (SP:A) was observed at -1.032 Å from the Hα line core with a total lifetime of ∼161.7 sec in the observed passband. The feature had a physical length of 3.8 Mm at an inclination of ∼21.4° over the observed limb, with apex-height reaching up to 5.3 Mm. Longitudinal motions in the Lagrangian frame were analyzed to estimate the velocity and duration of rise- and fall-phases, using a vertical slit (Fig. 1(a1) – (a4)) along the axis of spicule structure. Time-distance analysis of the vertical slit suggests a parabolic profile (Fig. 1(b)) of mass motions with an average ascending velocity of

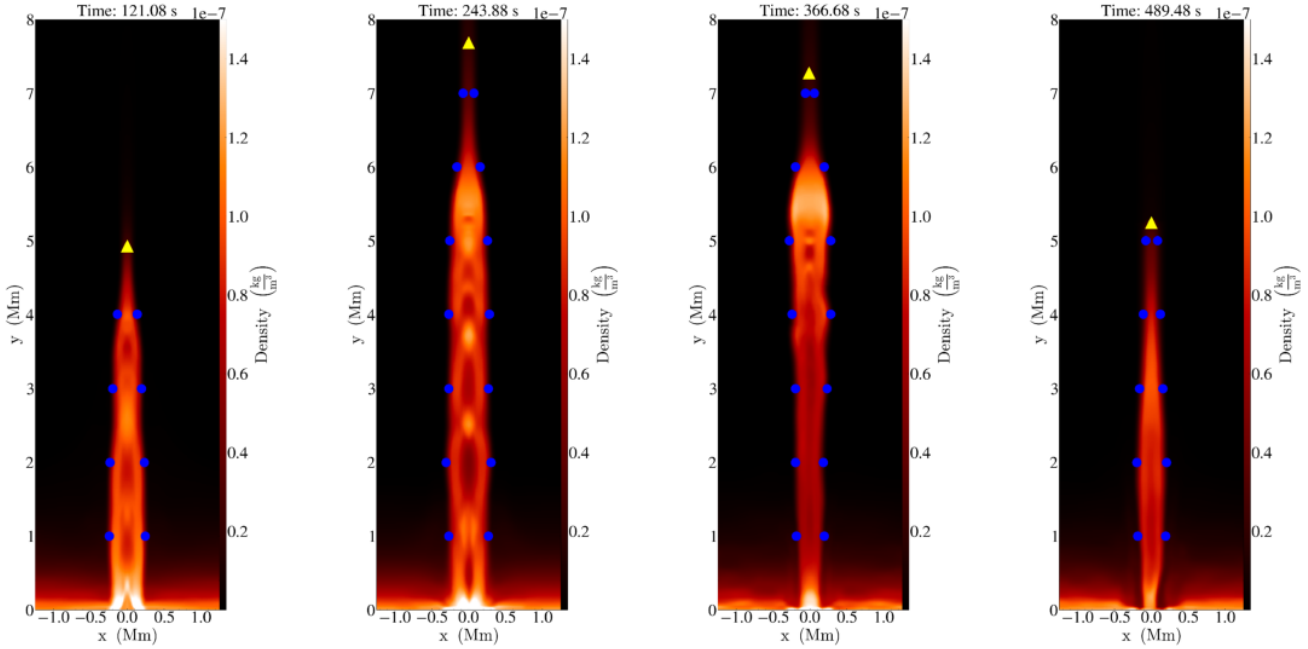

Figure 2. Panels showing the temporal evolution of the simulated spicule density structure at four time-steps with apex marked by a yellow triangle. From 121.08 − 243.88 s (366.68 − 489.48 s) the rising (falling)-phase Location of tracers edges are also shown as blue dots, which are used to estimate the variations in cross-sectional width during rise- and fall-phases of jet structure.

∼46.9 km/s. The plasma attains the maximum height in about 81 sec and then falls back to the surface with an average velocity of 40.2 km/s.

Cross-sectional widths were estimated at a height of ∼2 Mm above the visible limb location. For the observed lifetime, the average/unperturbed cross-sectional width estimate (W_u) for the spicule structure was around ∼176 km, which is comparable with other reports for off-limb spicules (Sharma et al. 2018). The temporal variations in cross-sectional width ($\delta W = W - W_u$) were used to estimate the periodicities in spectral domain and further comparison with simulations. The numerical setup for our study is chosen to highlight the fundamental dynamics of a chromospheric jet in a stratified atmosphere. Though the momentum-driven simulated jet lacks complex physical mechanisms, like e.g. radiative losses, ambipolar diffusion, ion-neutral effects, etc., it still mimics the crucial kinematic behavior, such as, longitudinal/field-aligned plasma motions with cross-sectional width variations (Fig. 2) in both rise- and fall-phase of the jet evolution.

The density structure of the simulated jet also shows complex internal substructures within the jet-beam, prominent during the rise-phase. Formation of these *knot*-like substructures appears to be concurrent with the structural deformations in the jet, and results due to high velocities at the jet footpoint. The *knot*-like features are a common ingredient to many astrophysical jets (Norman et al. 1982), and can arise due to a myriad of internal shock waves creating *crisscross/knot* pattern within the jet structure. The generation of these features has been routinely demonstrated in laboratory jets (Menon & Skews 2010; Edgington-Mitchell et al. 2014; Ono et al. 2014). **However, due to the limitations with spatial resolution of the current data set, this theoretically predicted fine structure inside the spicule jet cannot be verified from observations. The observed/simulated behavior could also be explained in terms of linear MHD theory as presence of either m=0 sausage and/or $m \geq$2 fluting wave modes. These two modes has common observational signatures that include concurrent cross sectional width and photometric variations. Previous studies (Jess et al. 2012; Morton et al. 2012; Gafeira et al. 2017) interpreted these observed behavior as presence of confined m=0 sausage wave modes in chromospheric jets, which could be misleading. However, existence of *knot-like* substructures from numerical simulations, here, provide an alternate possibility for the generation of cross sectional deformations in chromospheric jets, other than conventional MHD wave interpretations.**

Cross-sectional width estimates from both observations and numerical simulations indicate an oscillatory pattern during the feature's lifetime (Fig. 3, Sim:1.1, Obs:1.1). These periodic variations were further analyzed to estimate the dominant frequencies in the oscillations during the rise- and fall-phase of the jet evolution. Peak frequencies were identified in the wavelet analysis as spectral-magnitudes in WPS with significance levels over unity and higher, highlighted as black contours in

Figures 3. Furthermore, the peaks also had GPS over two-σ (95%) confidence levels (orange dashed-line in Fig. 3). Wavelet spectra for observed width variations during spicule lifetime, suggest a strong spectral density concentration around ∼17 sec for 5 cycles. Interestingly, for the simulated jet structure, the WPS indicates the presence of harmonics, concentrated around ∼65 sec and ∼32 sec for 8 and 5 cycles, respectively.

The effects of mass motions on the spicule becomes clear with the wavelet spectrum for both observed and simulated width estimates during their rise and fall intervals. The cross-sectional width oscillations show remarkable differences in their periodicities estimated when plasma is ascending along the magnetic field, against the gravity (rise-phase), and later tracing the field lines under the influence of gravity (fall-phase). Wavelet transforms for observational width variations indicate ∼27 sec periodicity for 3 cycles while a powerful 70 sec periodicity is present in both GPS and WPS of the simulation data. However, there is a noticeable shift towards lower/higher periodicities/frequencies, for two out of three of our identified spicule cases (Table 1), during the fall-phase of the plasma flows in the jet structure. Wavelet spectrum for observed width variations show dominant periodicity at 16 sec for 5 cycles while for simulated data, there are two strong periods, concentrated around ∼30 sec and ∼68 sec, each persistent for 5 and 2.5 cycles. These results are consistent with previous reports for cross-sectional width oscillations in on-disk fibrils (Gafeira et al. 2017).

An important aspect of our investigation is the confirmation of a first overtone in cross-sectional width periodicities associated with dynamic waveguides (spicules) in the solar chromosphere. Earlier studies were able to only identify higher harmonics in static waveguides (e.g., in a coronal loop), with the presence of fundamental and first overtone (Verwichte et al. 2004; Guo et al. 2015). Recently, the presence of a second overtone was also reported for coronal loop observations by Duckenfield et al. (2019), associated with transverse kink oscillations. It must be noted that wave harmonics can provide vital clues regarding plasma and magnetic field characteristics of the waveguide via solar magneto-seismology applications (Andries et al. 2005, 2009). The presence of overtones in jets provides a key tool for chromospheric magneto-seismology.

4. CONCLUSIONS

In this Letter, the dynamic response of field-aligned mass flows **on cross sectional width variations** within chromospheric jets is investigated. High-resolution CRISP/SST Hα data were used to identify **structural deformations** in off-limb spicules, complemented with analysis of a 2D numerical simulation for jets in a stratified solar atmosphere. Cross-sectional width estimates for both observed and simulated jets **indicate periodic oscillatory patterns suggest possible presence of linear MHD sausage/fluting wave modes and/or internal shocks**. Further, wavelet transform of time series cross-sectional widths show affects of plasma flows on estimated periods. Major conclusions of our investigation are as follows.

1. **Cross-sectional width variations in observed and simulated jets highlight the observed behavior as a fundamental property of spicule jets. Earlier reports interpreted these variations as a consequence of confined sausage waves in chromospheric jet structures, though similar characteristics are also shown by MHD fluting wave modes. Here, for the first time, an alternate explanation is provided in terms of internal shock/*knot-like* substructures for cross sectional deformations of chromospheric waveguides. Furthermore, it should be noted that this intrinsic/dynamic physical characteristic of jets is well established in astrophysical/laboratory studies, however, lacked attention for solar jets, primarily due to observational/instrumental constraints.**

2. **Spectral analysis using wavelet transform suggests noticeable modulation in estimated periodicities for the cross-sectional width variation in both observed and simulated jet structure. In most cases, periodicities tend to shift towards lower magnitudes during the fall-phase of the plasma in the jet, as compared to momentum-pulse driven rise-phase. Similar effects were reported in past for changes in linear MHD wave characteristics due to mass flows in theoretical and prominence studies.**

3. For the first time, the first overtone in the estimated periodicity is identified in both observed and simulated dynamic chromospheric waveguide (spicule). This could have important implications for chromospheric magneto-seismology, further enabling the estimation of much needed longitudinal plasma and magnetic field information for chromospheric jets.

Our study indicates the possible coupling between the longitudinal mass motions and **cross sectional width variations** in spicule structures. Understanding of such behavior is crucial for the accurate estimation of overall energy budget and associated dissipation mechanisms. Furthermore, simulations suggests the formation of *knot*-like substructures within the jet beam, prevalent during the rise-phase of plasma density. These substructures were closely linked with the estimated cross-sectional width variations in the jet and could possibly be generated due to superimposition of shock waves. Identification of signatures of any mode coupling

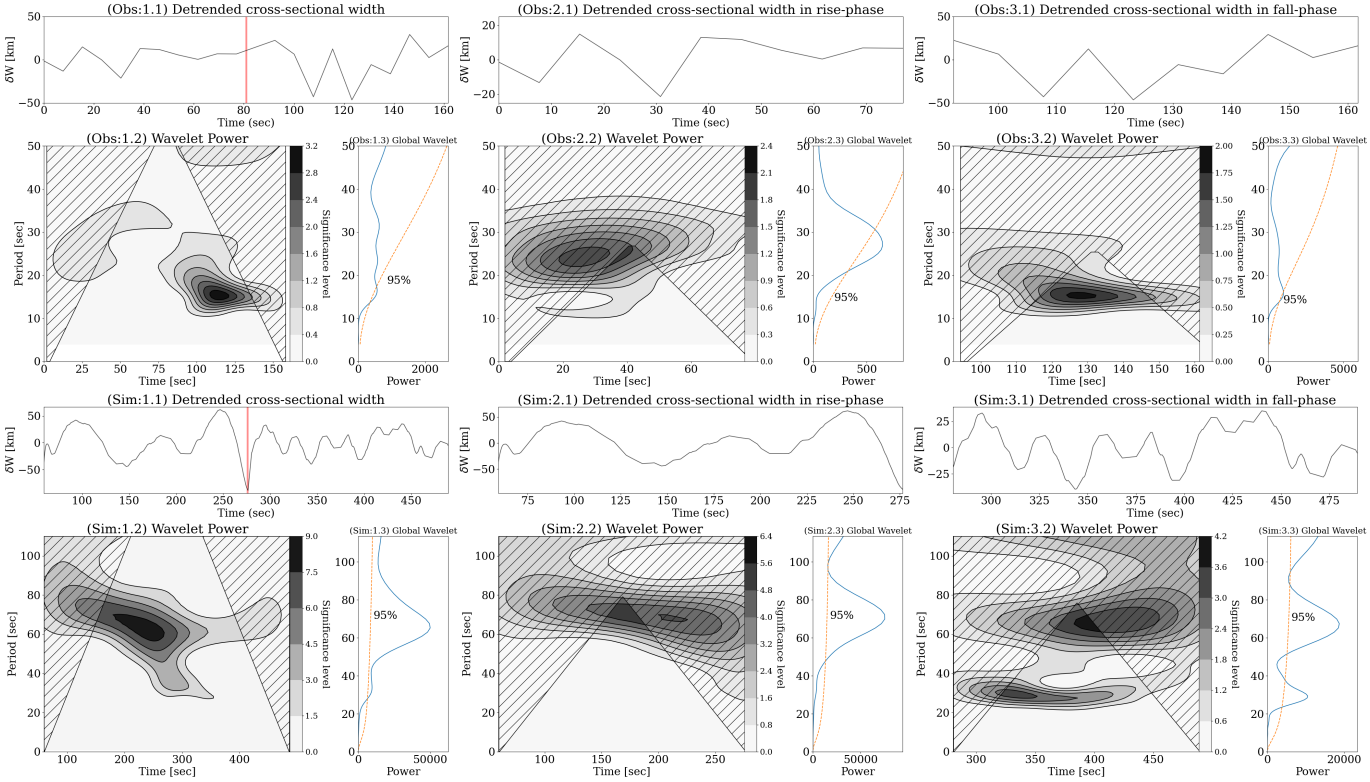

Figure 3. Panels showing the results of spectral analysis of cross-sectional width estimates of observed (top) and simulated (bottom) jet structures. Each panel depicts for temporal evolution of overall widths (1.1) and subsequent rise- (2.1) and fall-phases (3.1), along with Wavelet Power Spectra (WPS: 1.2, 2.2, 3.2) and Global Power Spectra (GPS: 1.3, 2.3, 3.3) during each phase of the evolution of the jet. Vertical red-line in plots (Obs: 1.1 and Sim 1.1) marks the time when the field-aligned plasma attained the apex height. Further, plots (Obs: 1.1, Sim: 3.2) provide clear indication of a second harmonic of the **cross-sectional width deformations** in the dynamic spicular waveguide.

and jet-substructures is foreseen in future studies using forthcoming Daniel K. Inouye Solar Telescope (DKIST) and European Solar Telescope (EST).

F.M., M.B.K and R.E acknowledge the support received from the Science and Technology Facilities Council (STFC) UK (grant numbers ST/S000518/1 at Aberystwyth University and ST/M000826/1 at the University of Sheffield). R.S. acknowledges support by the Spanish Ministry of Economy and Competitiveness (MINECO) through project AYA2016-80881-P (including FEDER funds). F.M is grateful for the STFC studentship and acknowledges the useful insights provided by M. Allcock. Part of the computations used Sheffield University HPC cluster ShARC. Numerical results used the open source software MPI-AMRVAC mainly developed at KU Leaven. The Swedish 1-m Solar Telescope is operated on the island of La Palma by the Institute for Solar Physics of Stockholm University in the Spanish Observatorio del Roque de los Muchachos of the Instituto de Astrofísica de Canarias. The Institute for Solar Physics is supported by a grant for research infrastructures of national importance from the Swedish Research Council (registration number 2017-00625).

REFERENCES

Andries, J., Arregui, I., & Goossens, M. 2005, ApJL, 624, L57

Andries, J., van Doorsselaere, T., Roberts, B., et al. 2009, SSRv, 149, 3

Beckers, J. M. 1972, ARA&A, 10, 73

Čada, M., & Torrilhon, M. 2009, Journal of Computational Physics, 228, 4118. http://www.sciencedirect.com/science/article/pii/S0021999109000953

Centeno, R., Trujillo Bueno, J., & Asensio Ramos, A. 2010, ApJ, 708, 1579

de la Cruz Rodríguez, J., Löfdahl, M. G., Sütterlin, P., Hillberg, T., & Rouppe van der Voort, L. 2015, A&A, 573, A40

De Pontieu, B., Carlsson, M., Rouppe van der Voort, L. H. M., et al. 2012, ApJL, 752, L12

De Pontieu, B., McIntosh, S. W., Carlsson, M., et al. 2007, Science, 318, 1574

Dedner, A., Kemm, F., Kröner, D., et al. 2002, Journal of Computational Physics, 175, 645. http://www.sciencedirect.com/science/article/pii/S002199910196961X

Duckenfield, T. J., Goddard, C. R., Pascoe, D. J., & Nakariakov, V. M. 2019, A&A, 632, A64

Ebadi, H., & Ghiassi, M. 2014, Ap&SS, 353, 31

Edgington-Mitchell, D., Honnery, D. R., & Soria, J. 2014, Physics of Fluids, 26, 096101. http://aip.scitation.org/doi/10.1063/1.4894741

Gafeira, R., Jafarzadeh, S., Solanki, S. K., et al. 2017, ApJS, 229, 7

Goossens, M., Soler, R., Terradas, J., Van Doorsselaere, T., & Verth, G. 2014, ApJ, 788, 9

Guo, Y., Erdélyi, R., Srivastava, A. K., et al. 2015, ApJ, 799, 151

Harten, A., Lax, P. D., & van. Leer, B. 1983, SIAM Review, 25, 35. https://doi.org/10.1137/1025002

Jess, D. B., Pascoe, D. J., Christian, D. J., et al. 2012, ApJL, 744, L5

Keppens, R., Meliani, Z., van Marle, A. J., et al. 2012, Journal of Computational Physics, 231, 718

Kukhianidze, V., Zaqarashvili, T. V., & Khutsishvili, E. 2006, A&A, 449, L35

Loughhead, R. E. 1974, SolPhys, 35, 55

Menon, N., & Skews, B. W. 2010, Shock Waves, 20, 175

Morton, R. J., Verth, G., Jess, D. B., et al. 2012, Nature Communications, 3, 1315

Nakariakov, V. M., & Roberts, B. 1995, SoPh, 159, 213

Narayanan, A. S. 1991, Plasma Physics and Controlled Fusion, 33, 333. https://doi.org/10.1088%2F0741-3335%2F33%2F4%2F005

Norman, M. L., Winkler, K. H. A., Smarr, L., & Smith, M. D. 1982, A&A, 113, 285

Ono, N., Yamamoto, M., & Koike, K. 2014, Vacuum, 110, 149

Pereira, T. M. D., De Pontieu, B., & Carlsson, M. 2012, ApJ, 759, 18

Pereira, T. M. D., De Pontieu, B., Carlsson, M., et al. 2014, ApJL, 792, L15

Porth, O., Xia, C., Hendrix, T., Moschou, S. P., & Keppens, R. 2014, ApJS, 214, 4

Rouppe van der Voort, L., Leenaarts, J., de Pontieu, B., Carlsson, M., & Vissers, G. 2009, ApJ, 705, 272

Ruderman, M. S., Goossens, M., & Andries, J. 2010, Physics of Plasmas, 17, 082108

Scharmer, G. B., Narayan, G., Hillberg, T., et al. 2008, ApJL, 689, L69

Sekse, D. H., Rouppe van der Voort, L., De Pontieu, B., & Scullion, E. 2013, ApJ, 769, 44

Sharma, R., Verth, G., & Erdélyi, R. 2017, ApJ, 840, 96

—. 2018, ApJ, 853, 61

Soler, R., Oliver, R., & Ballester, J. L. 2008, ApJ, 684, 725

Sterling, A. C. 2000, SoPh, 196, 79

Suárez, D. O., Ramos, A. A., & Bueno, J. T. 2015, The Astrophysical Journal, 803, L18. https://doi.org/10.1088%2F2041-8205%2F803%2F2%2Fl18

Terra-Homem, M., Erdélyi, R., & Ballai, I. 2003, SoPh, 217, 199

Torrence, C., & Compo, G. P. 1998, Bulletin of the American Meteorological Society, 79, 61

Tóth, G. 1996, Astrophysical Letters and Communications, 34, 245

Tsiropoula, G., Tziotziou, K., Kontogiannis, I., et al. 2012, Space Science Review, 169, 181

van Noort, M., Rouppe van der Voort, L., & Löfdahl, M. G. 2005, SolPhys, 228, 191

Verwichte, E., Nakariakov, V. M., Ofman, L., & Deluca, E. E. 2004, SoPh, 223, 77

Xia, C., Teunissen, J., El Mellah, I., Chane, E., & Keppens, R. 2017, ArXiv e-prints, arXiv:1710.06140

Zaqarashvili, T. V., & Erdélyi, R. 2009, Space Science Review, 149, 355

Ziegler, U., & Ulmschneider, P. 1997a, A&A, 324, 417

—. 1997b, A&A, 327, 854

APPENDIX

A. EXTRA MATERIAL

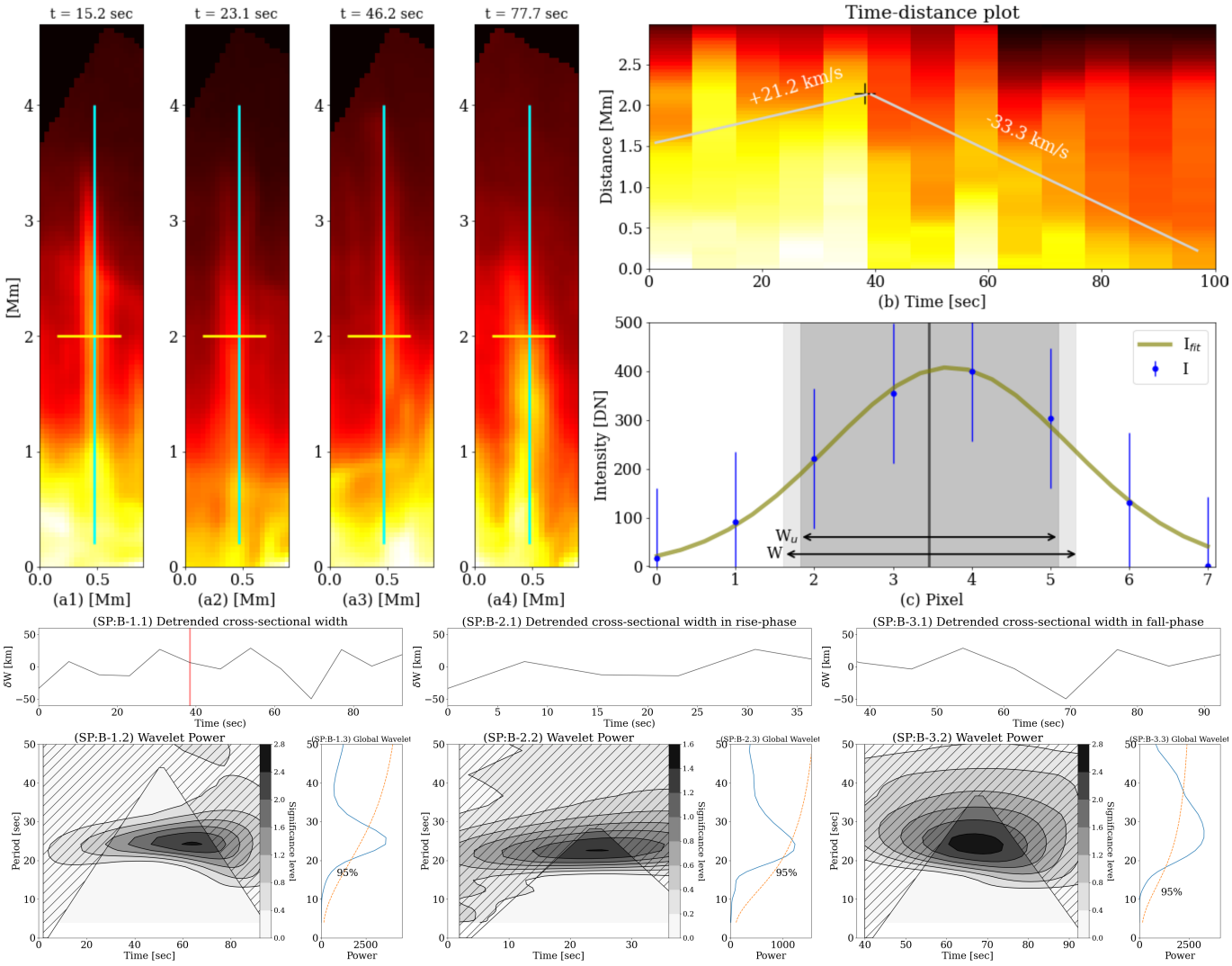

Figure 4. Spicule SP:B, with similar details as described in caption of Figures 1 and 3

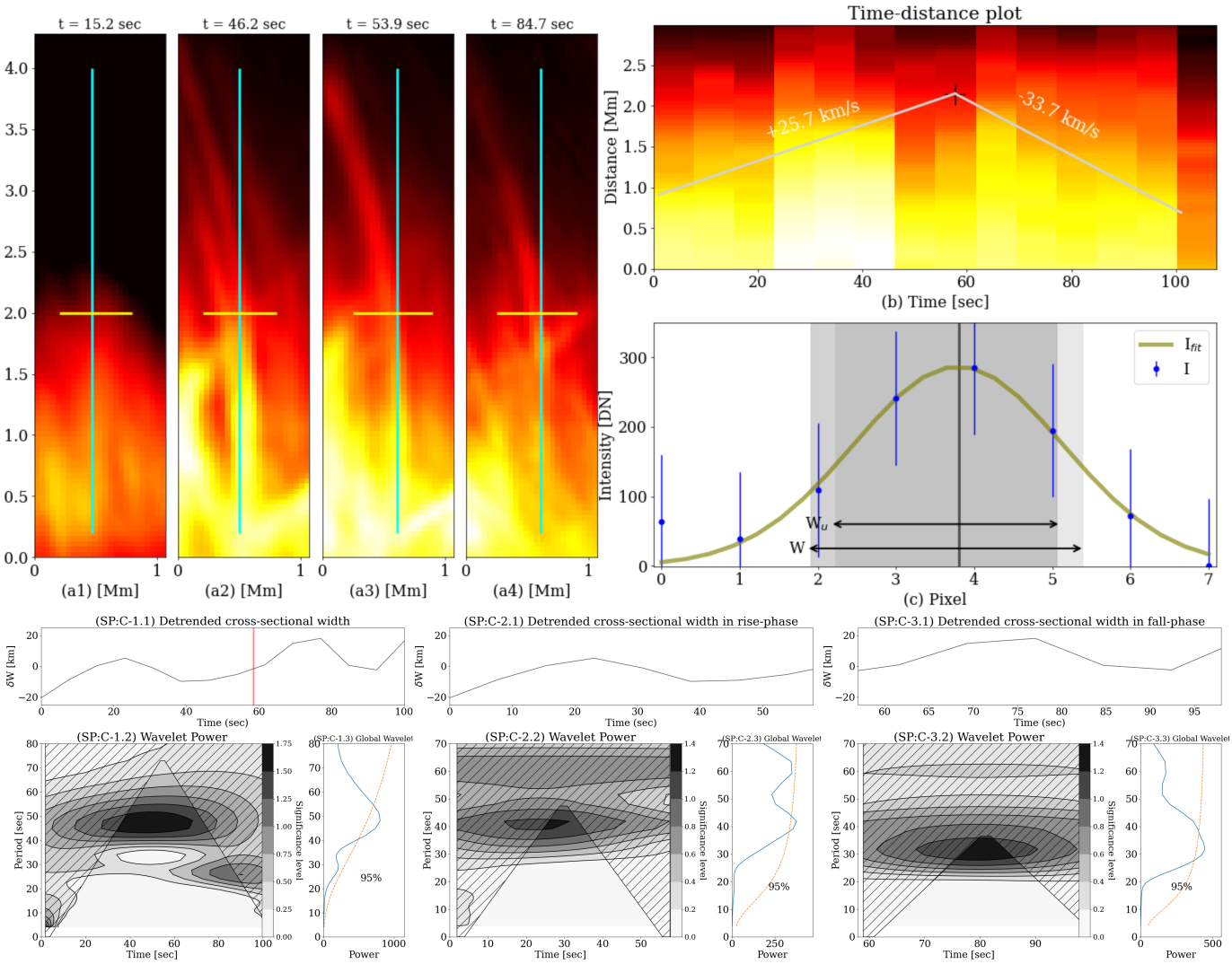

Figure 5. Spicule SP:C, with similar details as described in caption of Figures 1 and 3